Revealing the Orbital Composition of Heavy Fermion Quasiparticles in CeRu<inf>2</inf>Si<inf>2</inf>

Journal of the Physical Society of Japan **92**, 104701 (2023)
https://doi.org/10.7566/JPSJ.92.104701

Revealing the Orbital Composition of Heavy Fermion Quasiparticles in $CeRu_2Si_2$

Kevin P. Kramer[1], Rina Tazai[2], Karin von Arx[1], Masafumi Horio[1], Julia Küspert[1], Qisi Wang[1], Yasmine Sassa[3], Timur K. Kim[4], Céphise Cacho[4], Julien E. Rault[5], Patrick Le Fèvre[5], François Bertran[5], Marc Janoschek[1,6], Nicolas Gauthier[7,8], Daniel Mazzone[9], Ramzy Daou[10], and Johan Chang[1]

[1]*Physik-Institut, Universität Zürich, Winterthurerstrasse 190, CH-8057 Zürich, Switzerland*
[2]*Department of Physics, Nagoya University and JST, TRIP, Nagoya 464-8602, Japan*
[3]*Department of Physics, Chalmers University of Technology, SE-412 96 Göteborg, Sweden*
[4]*Diamond Light Source, Harwell Campus, Didcot, OX11 0DE, United Kingdom*
[5]*Synchrotron SOLEIL, Saint-Aubin-BP 48, F-91192 Gif sur Yvette, France*
[6]*Laboratory for Neutron and Muon Instrumentation, Paul Scherrer Institut, CH-5232 Villigen PSI, Switzerland*
[7]*Stanford Institute for Materials and Energy Sciences, SLAC National Accelerator Laboratory and Stanford University, Menlo Park, California 94025, U.S.A.*
[8]*Institut Quantique, Département de Physique, Université de Sherbrooke, Sherbrooke, Québec J1K 2R1, Canada*
[9]*Laboratory for Neutron Scattering and Imaging, Paul Scherrer Institut, 5232 Villigen PSI, Switzerland*
[10]*Normandie Univ, ENSICAEN, UNICAEN, CNRS, CRISMAT, Caen, France*

(Received November 14, 2022; accepted July 27, 2023; published online September 5, 2023)

We present a resonant angle-resolved photoemission spectroscopy (ARPES) study of the electronic band structure and heavy fermion quasiparticles in $CeRu_2Si_2$. Using light polarization analysis, considerations of the crystal field environment and hybridization between conduction and *f* electronic states, we identify the *d*-electronic orbital character of conduction bands crossing the Fermi level. Resonant ARPES spectra suggest that the localized Ce *f* states hybridize with e_g and t_{2g} states around the zone center. In this fashion, we reveal the orbital structure of the heavy fermion quasiparticles in $CeRu_2Si_2$ and discuss its implications for metamagnetism and superconductivity in the related compound $CeCu_2Si_2$.

1. Introduction

The term *heavy fermions* refers to electronic quasiparticles (QPs) with a strongly renormalized mass compared to free electrons. Hybridization between localized *f*-electronic states and conduction electrons is a pathway for heavy fermion formation. These QPs are the starting point for a plethora of exotic quantum matter states. Superconductivity,[1)] magnetism and multipole ordered[2,3)] phases have been realized in this fashion. Very often, these phases are highly sensitive to external tuning parameters such as pressure or magnetic fields. Two superconducting phases have, for example, been identified as a function of hydrostatic pressure in $CeCu_2Si_2$.[4)] The symmetry of the superconducting order parameters is still being debated. The very same material also has a so-called A-phase that is magnetically ordered.[5)] Another example is URu_2Si_2 that also hosts an unconventional superconducting state inside a hidden-order phase with an unresolved symmetry breaking.[6–8)] These phases vanish upon application of magnetic field and are replaced by a magnetic ground state. Here, we consider $CeRu_2Si_2$ that undergoes a metamagnetic transition at a magnetic field of just 7 T. On both sides of the transition, the QP masses inferred from quantum oscillation experiments only account for 20% of the observed electronic specific heat.[9,10)] The heavy fermion Fermi surface structures have therefore not been detected by quantum oscillation experiments.

It is commonly believed that the heavy fermion QPs are a dominant factor in these materials' low-energy electronic structures and responsible for the highly tunable phase diagrams. A profound characterization of the QP nature is therefore desired. Resonant angle-resolved photoemission spectroscopy (ARPES), applied across a wide selection of Ce-based compounds, has provided insight into the *f*-electronic spectral weight folded into low-energy QPs.[11–22)] By tuning the incident photons to the Ce-Fano-resonance, sensitivity to *f*-electronic spectral weight is enhanced. In this fashion, the *f*-electron contribution to the QPs residing on the Fermi surface is probed. Yet, the orbital composition of these QPs remains difficult to disentangle. In the case of $CeRu_2Si_2$ and related 122-compounds, the localized *f* states split into two levels, $f_{5/2}$ and $f_{7/2}$, due to spin–orbit coupling (SOC). Their degeneracy is lifted further through the tetragonal crystal electric field (CEF).[22)] The $f_{5/2}$ state therefore splits into the three levels labeled Γ_7^1, Γ_7^2, and Γ_6. Moreover, the conduction electrons can have both *d* and *p* orbital character. Without taking strong electron interaction and SOC into account, band structure calculations are typically not reliable in these compounds. The orbital structure of the heavy fermions is therefore difficult to access from both experimental and theoretical view points.

Here we use a combination of resonant and light polarization dependent ARPES to elucidate the orbital structure of the heavy fermions in $CeRu_2Si_2$. In contrast to several previous ARPES studies,[23,24)] we probe the Ce 121 eV Fano resonance[25,26)] using high-resolution instrumentation. On both Si- and Ce-terminated surfaces, strong hybridization between localized *f* states and conduction bands (*cf* hybridization) is found around the zone center. The low-temperature *f*-electron spectral weight is suppressed above $T \approx 25$ K. By exploiting the photoemission matrix element's dependence on light polarization, we infer that the *cf* hybridization occurs predominately with the $d_{3z^2-r^2}$ and d_{xz}, d_{yz} ruthenium orbitals.

2. Methods

High quality single crystals were grown using the Czochralski technique and have previously been used for

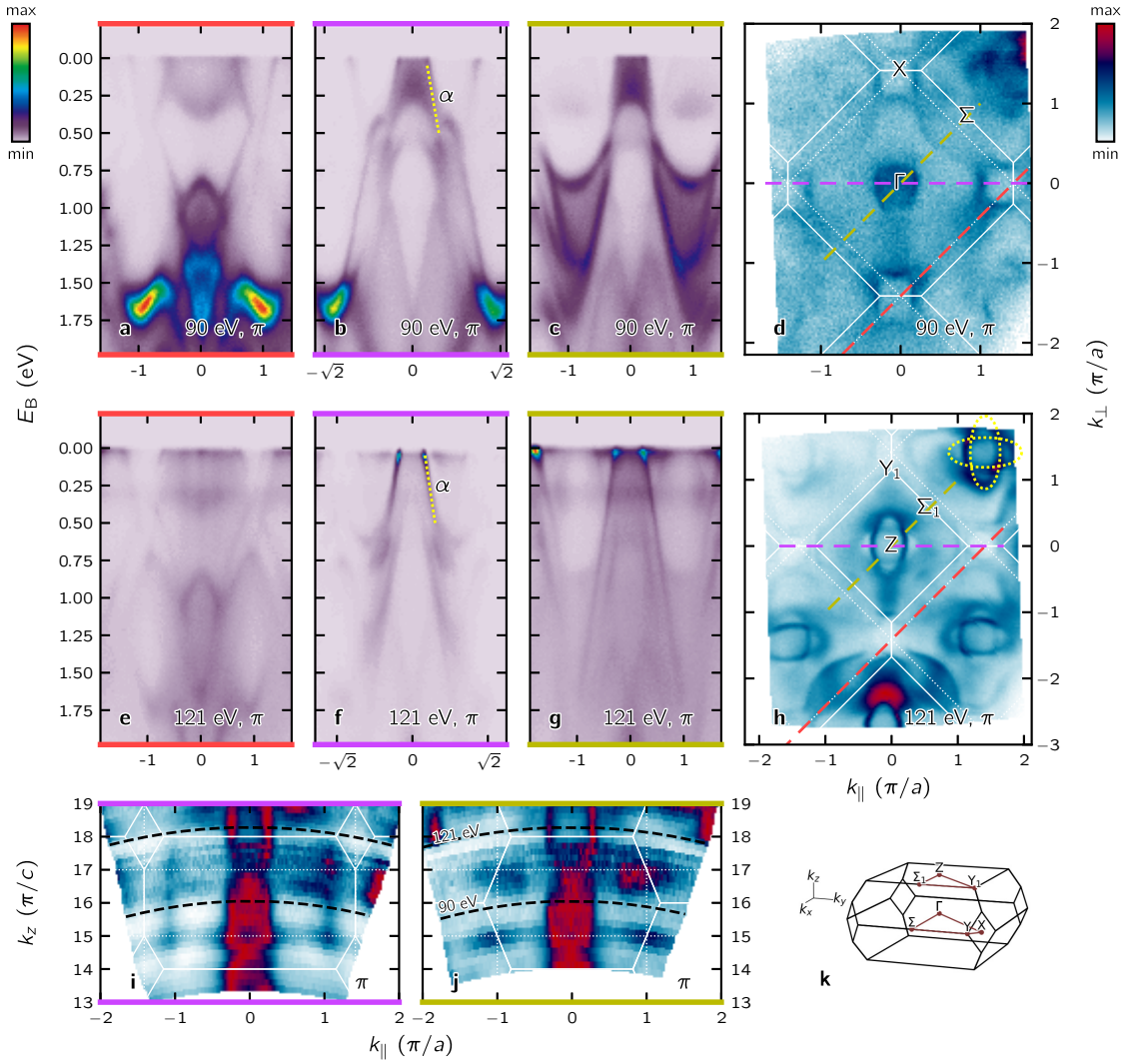

Fig. 1. (Color online) High-symmetry band structure and Fermi surface from a Ce-terminated surface. The first and second rows are recorded using photons tuned to be off- or on-resonance, respectively. Under both conditions, the band structure along high symmetry directions is displayed in (a)–(c) and (e)–(g). On- and off-resonance Fermi surface maps were recorded at 13 K (d, h). Colored dashed lines indicate the high-symmetry trajectories along which the band structure is displayed in (a)–(c) and (e)–(g). Panels (i) and (j) show the Fermi surface along the k_z direction for cuts along ΓX and ΓΣ, respectively. White lines in (d, h, i, f) indicate the body-centered tetragonal Brillouin zone boundaries. Simple tetragonal Brillouin zone boundaries are also shown with dotted white lines. A schematic of the body-centered tetragonal Brillouin zone with the locations of the special points is shown in panel (k). Panels displaying data recorded with same incident photon energy share a common color scale normalization.

magneto-resistance measurements.[9,10] ARPES experiments were carried out at the Cassiopee and I05[27] beam lines at the Soleil synchrotron and the Diamond Light Source, respectively. The crystals were cleaved using a standard top-post. Electrical contact between the crystal and the cryostat was obtained using EpoTek H20E Ag epoxy. Incident photon energies 90 eV (off-resonance) and 121 eV (on-resonance) were used in combination with horizontal π and vertical σ linear light polarizations. A vertical analyser slit configuration was used throughout this work. We denote k_x and k_y in units of π/a and k_z in units of π/c with $a = 4.95$ Å and $c = 9.798$ Å being the lattice parameters. Assuming an inner potential $V_0 = 15$ eV as is commonly used for d-electron systems,[28–30] our momentum mapping at the Ce-resonance is close to $Z = (0, 0, 1)$ and $Y_1 = (1, 1, 1)$. By contrast, for $h\nu = 90$ eV, the in-plane mapping is cutting close to $\Gamma = (0, 0, 0)$ and $\Sigma = (1, 1, 0)$ points. Data analysis and visualization was carried out using the PIT software package.[31] Data has been normalized to the average background count rate found above the Fermi level. Surface terminations (Si or Ce) are distinguished through the same considerations as in related 122 compounds.[11]

3. Results

On- and off-resonance ARPES spectra collected along high symmetry direction on a Ce-terminated surface, shown in Figs. 1(a)–1(c) and 1(e)–1(g), reveal a rich band structure. Numerous dispersive bands are observed along with the non-dispersive Ce $4f_{7/2}$[11,22] state at a binding energy of roughly 0.3 eV [best seen in Fig. 1(g)]. The associated on- and off-resonance Fermi surfaces perpendicular to k_z are displayed in Figs. 1(d) and 1(h), while Fermi surfaces parallel to k_z along the high symmetry directions ΓX and ΓΣ are shown in Figs. 1(i) and 1(j), respectively. From panels (d) and (h) it is apparent that the X-point exhibits 4-fold symmetry, in contrast to previous reports where this point has 2-fold symmetry.[23,26] The dotted outline of the simple tetragonal Brillouin zone (BZ) boundaries are a better match for the

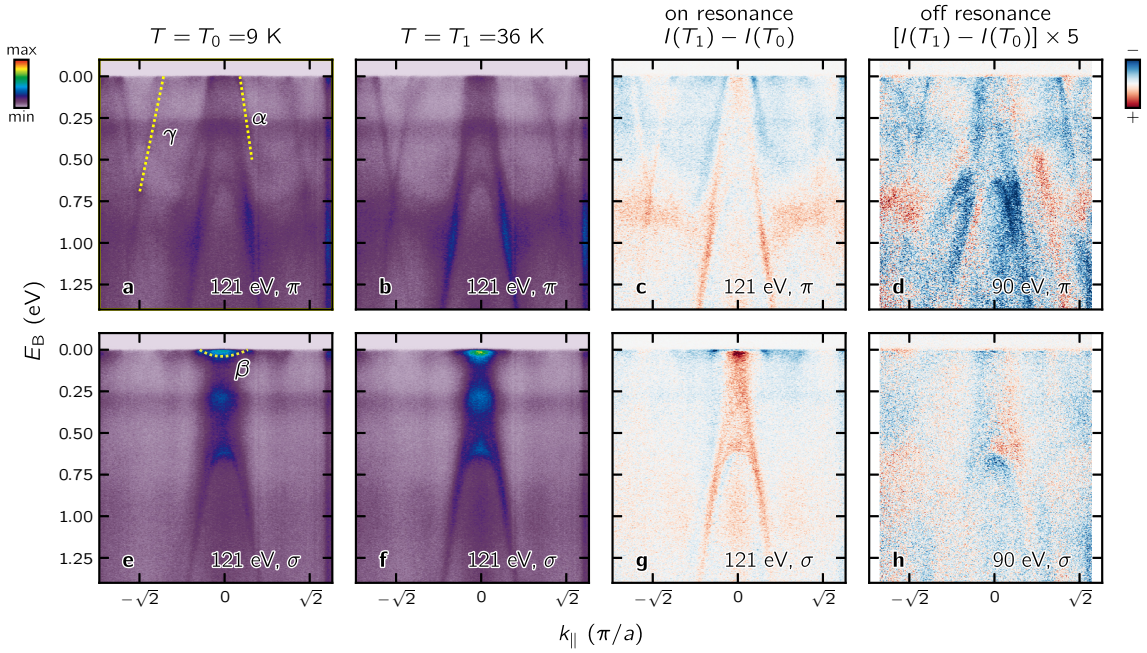

Fig. 2. (Color online) Zone corner band structure from Si-terminated Fermi surface. (a, b), (e, f) Band structure along the Z-Y_1 directions recorded with linear horizontal (π) and vertical (σ) light polarization for temperatures as indicated. (c, d), (g, h) Intensity difference I(36 K)–I(9 K) for the two polarizations at the resonance and off-resonance. The color scale is organized so that white indicates no difference, red indicates intensity gain and blue intensity loss upon heating. The color scale of the off resonance difference spectra (d, h) has been enhanced by 500% in order to make features visible at all. On the resonance, loss and gain traces the band structure whereas the off-resonance differences are generally a factor of 5 weaker and appear rather random.

measured data than the more appropriate body-centered tetragonal BZ boundaries. Further discussion on this observation can be found in the supplemental material.[32] In the following, we conclude from this observation that the data obtained on- and off-resonance is directly comparable in terms of band structure.

Several Fermi surface sheets can be identified. A small electron pocket [labeled γ in Fig. 2(a)] is found around the Y_1-point. Around the zone center, Z, a small (α) and a slightly larger (β) Fermi surface sheet are observed. They form the inner part of a flower-like shape, indicated with a dotted line in Fig. 1(h). The smaller α Fermi surface sheet displays a pronounced enhancement under resonant illumination, compare Figs. 1(b) and 1(c) with Figs. 1(f) and 1(g). This resonance effect implies that *f*-electronic spectral weight is folded into the low-energy QPs. The orbital nature of these composed QPs is our central point of focus here.

When rare earth ions are surrounded by Si layers the chemical surrounding resembles that of the bulk.[11,33] In principle, by addressing the Si-terminated surface we ensure that the observed *f*-electron physics represents the bulk properties, rather than those of surface Ce atoms. Surface effects are, however, commonly observed in related systems. In particular, the absent k_z dispersion of the α band [apparent from Fig. 1(i)] is reminiscent of previous reports,[34–36] where the k_z dispersion is affected by surface effects. We note that even if we are observing strong k_z broadening or a surface projection of the bulk electronic state, the agreement with soft x-ray ARPES data[23] makes it clear that the observed bands emerge from the same orbitals as the corresponding bulk states [compare panels b, f, d, and i of Fig. 1 to the respective figures in the x-ray ARPES report:[23] Figs. 2(b), 2(a), 4(a), and 4(b)].

Band structure along the Z-Y_1 direction is systematically collected with on- and off-resonance, σ and π light polarization, and as a function of temperature up to 36 K (Figs. 2 and 3). The on-resonance data displayed in Figs. 2 and 3 exhibits a clear temperature dependence around the Fermi level. Here band structure changes as a function of temperature seem to occur [Figs. 2(c), 2(d), 2(g), 2(h), and 3]. We also notice that the spectral weight of the conduction bands seems to change even far from the Fermi level [Figs. 2(c) and 2(d)]. The off-resonance data by contrast display little or no temperature dependence [Figs. 2(d) and 2(h)], as expected. Altogether, this suggests that the observed resonant temperature dependence is associated with the *cf* hybridization, which is known to have a thermal dependence due to the Kondo effect. It can however not be excluded that the temperature effect at large binding energy is linked to resonant photoemission effects.

The γ-band forms a Dirac-cone like structure around the Y_1-point. This band is only observed in the π channel and vanishes when σ polarization is used [see Figs. 2(a) and 2(e)]. The direct implication is that this band has even orbital character with respect to the photoemission mirror plane.[37,38] We also stress that this band does not display any significant resonance effects. It does therefore not seem to hybridize with the *f*-electronic states. Furthermore, it should be pointed out that we do not observe any k_z dispersion for the γ-band [Fig. 1(i)]. This, like the previously mentioned discrepancy in the symmetry of the X point, is again in contrast to previous reports,[23,26] where the corresponding band shows a small but appreciably dispersion along k_z.

The band structure around the zone center (Γ- and Z-points) also displays a strong dependence on light polarization, on/off resonance condition and temperature. With π

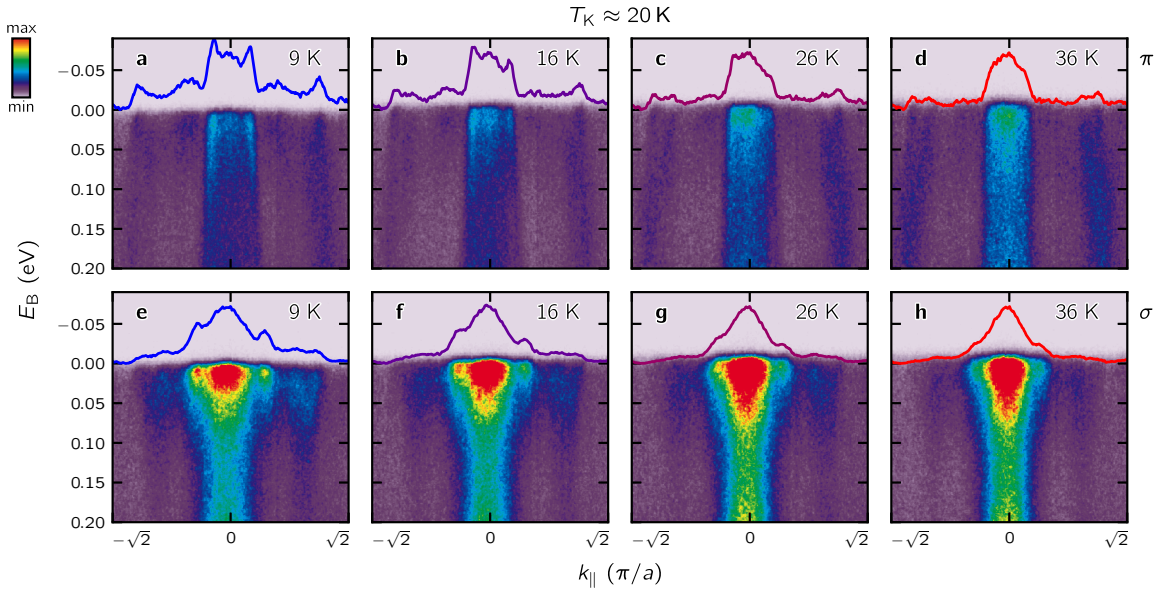

Fig. 3. (Color online) Temperature dependence of quasiparticles. Energy distribution maps recorded on the Ce-resonance along the Z-Y_1 direction for different temperatures. Top (bottom) panels are recorded with π (σ) light polarization. Solid lines are momentum distribution curves, integrated over a binding energy (E_B) range from 30 to 0 meV. The intensity of these curves is normalized to their values at the Y_1-point.

polarization, a hole-like band structure (labeled α) is found at the lowest measured temperature. By contrast in the σ channel an electron-like structure accompanied with two resonance structures are observed around the Z-point [Figs. 2(a) and 2(e)]. Both the hole-like structure and the resonances found in the π and σ channels, respectively, are weakened in spectral weight as temperature is increased [Figs. 2(c), 2(g), and 3]. These are the observations that we are going to use in the following to elucidate the orbital nature of the *cf*-composed QPs.

4. Analysis

We now turn to an analysis of the *cf* hybridization that is dictated by symmetry and extent of orbital overlap. Generally, the conduction electrons can hybridize with the $f_{5/2}$ states. In a tetrahedral crystal field they split into three levels: $\Gamma_7^1 = a|J_z = \pm 5/2\rangle + b|J_z = \mp 3/2\rangle$, $\Gamma_6 = |J_z = \pm 1/2\rangle$, and $\Gamma_7^2 = a|J_z = \mp 3/2\rangle - b|J_z = \pm 5/2\rangle$ with $a^2 + b^2 = 1$. X-ray absorption spectroscopy and inelastic neutron scattering studies yield $|a| = 0.8$ for $CeRu_2Si_2$.[39] The sign of a has not been determined experimentally but is established to be negative in $CeCu_2Si_2$, with a similar absolute value.[39] In what follows, we assume that $CeCu_2Si_2$ and $CeRu_2Si_2$ both have $a < 0$ even though $a > 0$ has previously been used in theoretical literature.[4] Since the conduction bands display strong light polarization dependence, they must have significant even and odd orbital character with respect to the photoemission mirror plane. The in-plane Si p orbitals do not have the respective symmetries, along the projected unit cell diagonal. Furthermore, in $LaRu_2Si_2$, the low-energy electronic structure predominately stems from the ruthenium d-orbitals.[40] In what follows, we assume that this conclusion extends to $CeRu_2Si_2$. Consequently, we are considering hybridization integrals between Ru d orbitals and $f_{5/2}$ states.

The tetrahedral crystal field environment splits the Ru d-orbitals into e_g ($d_{x^2-y^2}$ and $d_{3z^2-r^2}$) and t_{2g} ($d_{xy}, d_{xz} + d_{yz}, d_{xz} - d_{yz}$) states with e_g being energetically favorable.

Table I. Symmetry and *cf* hybridization overlap integrals. (Top) The parity with respect to the diagonal mirror plane of the different d orbitals is given in the second column. The remaining columns show the values of k-dependent overlap integrals $|\langle d|f\rangle|$, with $f \in \{\Gamma_6, \Gamma_7^1, \Gamma_7^2\}$ at the Z point in units of the coupling parameter $t_{df\sigma}$ for $k_z = 1$. (Bottom) Parity along the diagonal for the bands α, β, and γ. Observation of hybridization with localized f-electrons is indicated by yes or no. The last column indicates the intensity ratio between $T_0 = 9$ K and $T_1 = 36$ K.

Orbital	Parity ($k_x = k_y$)	$\|\Gamma_6\rangle$	$\|\Gamma_7^1\rangle$	$\|\Gamma_7^2\rangle$
$\langle x^2 - y^2\|$	odd	0	0.24	1.0
$\langle z^2\|$	even	0.16	0	0
$\langle xy\|$	even	0	0	0
$\langle xz + yz\|$	even	0.57	0.12	0.58
$\langle xz - yz\|$	odd	0.57	0.12	0.58

Label	Parity ($k_x = k_y$)	Hybrid.	$I(T_0)/I(T_1)$
α	even	yes	≈2
β	odd	yes	≈2
γ	even	no	1

The Ru atoms are found at a mixed valence of Ru^{2+} and Ru^{3+}, which correspond to $4d^6$ or $4d^5$ electronic configurations. Combined, these two facts imply fully (partially) occupied e_g (t_{2g}) states. The e_g states $d_{x^2-y^2}$ and $d_{3z^2-r^2}$ have, respectively, odd and even parity along the diagonals Γ-Σ and Z-Y_1. In the t_{2g}-sector, d_{xy} is even whereas d_{xz} and d_{yz} display mixed character. However, the linear combination $d_{xz} + d_{yz}$ is even while $d_{xz} - d_{yz}$ is odd along Γ-Σ.

We are now ready to make our first conclusions. The γ band around the Y_1-point displays even character and no significant resonance effect. This band does therefore not hybridize with the localized f-states. By evaluating $\langle d|\Gamma_7^1\rangle$ and $\langle d|\Gamma_7^2\rangle$, we find that only d_{xy} is consistent with this observation within σ-coupling,[41,42] i.e., only $\langle d_{xy}|\Gamma_7^1\rangle = \langle d_{xy}|\Gamma_7^2\rangle = 0$ (see Table I). The absent hybridization of Ru d_{xy} with the Ce f states is intuitively sound from geometric considerations. The spatial extent of the d_{xy}

orbitals at the Ru sites is directed towards the neighbouring Ru atoms, prohibiting hybridization with Ce f states for symmetry reasons.

The β band around the Z-point completely disappears under π illumination. We can therefore assign odd orbital character to this band and thus, the orbitals $d_{x^2-y^2}$ or $d_{xz} - d_{yz}$ are the only possibilities. Given the tetrahedral crystal field environment, partial filling of $d_{xz} - d_{yz}$ is expected. Hence, the β band is most likely composed of $d_{xz} - d_{yz}$ orbital character. The α band is hole-like and located around the zone center. It disappears completely in the σ channel, implying even mirror symmetry. Arguing again with partial occupation of the t_{2g} states, the α band therefore most conceivably has $d_{xz} + d_{yz}$ character.

Figure 3 presents a more detailed view of the temperature effect shown in Figs. 2(c), 2(d), 2(g), and 2(h). Both from the spectra and the momentum distribution curves it becomes clear that the α and β features selectively lose spectral weight when the temperature is increased beyond this system's Kondo temperature T_K of around 20 K.[43,44] This is the expected behaviour for Kondo QPs as the coupling between localized and itinerant states becomes weak above T_K, leading to their break up.

5. Discussion

The observation of cf hybridization around the zone corner is not consistent with previous interpretations of Compton scattering experiments on $CeRu_2Si_2$.[45] As a function of temperature across T_K Compton scattering data has been read in terms of Fermi surface changes around the zone corner.[45] We also notice that superconducting $CeCu_2Si_2$ with similar crystal field environment displays strong zone-corner cf hybridization with an overall different Fermi surface structure.[46]

It is commonly believed that tunable phases of $CeCu_2Si_2$ (superconductivity) and $CeRu_2Si_2$ (metamagnetic transition) are rooted in the heavy fermion QPs formed by the cf hybridization. In principle, both unconventional superconductivity and field-induced metamagnetic transitions have been observed in d-electron systems without Kondo physics.[47,48] For the case of metamagnetic transitions, for example in the ruthenates, they involve large density of states (DOS).[49] In $Sr_3Ru_2O_7$ and $Ca_{1.8}Sr_{0.2}RuO_4$ the large DOS is reached by tuning a d_{xy}-dominated van Hove singularity.[50] In $CeRu_2Si_2$, by contrast, the d_{xy} band is not carrying any van Hove singularity and does not hybridize with the flat f states. Hence, it is unlikely to be involved in the metamagnetic transition. Instead, the $\langle d_{xz} - d_{yz}|\Gamma_7\rangle$ and $\langle d_{xz} + d_{yz}|\Gamma_7\rangle$ QPs are more likely candidates. Especially, the $\langle d_{xz} - d_{yz}|\Gamma_7\rangle$ QP appears as a very shallow band around the zone center and hence should carry significant DOS. The $\langle d_{xz} - d_{yz}|\Gamma_7\rangle$ QPs are therefore far more likely to be involved in the metamagnetic transition.

We close the discussion with a remark on the relative hybridization overlaps with the Γ_7^1 and Γ_7^2 states. The hybridization overlaps with Γ_7^2 have been found to be larger than those of Γ_7^1 (Table I). In $CeCu_2Si_2$, the ratio of occupancies of these two states is expected to flip in favor of Γ_7^2 with increasing temperature over the measured range.[4] If we were to assume that the same holds true for $CeRu_2Si_2$, higher occupancy of Γ_7^2 would thus imply more hybridized states at higher temperatures. This is at odds with the observation. However, this would most likely simply be due to the fact that the coupling leading to Kondo QP formation above T_K is so weak that the increased hybridization overlap does not have any noticeable influence.

6. Conclusion

In summary, we have carried out a high resolution on- and off-resonance ARPES study of $CeRu_2Si_2$. The resonance ARPES data suggest cf hybridization to occur predominately around the zone center. Using light polarization analysis, and considerations of crystal field environment the d-orbital character of the conduction bands have been inferred. Theoretical evaluation of the hybridization in combination with experimental temperature dependence led to a unique QP structure determination. The cf hybridization stems predominately from hybridization of $d_{3z^2-r^2}$ and d_{xz}, d_{yz} ruthenium orbitals. On this basis, implications for metamagnetism have been discussed.

Acknowledgments K.P.K., M.H., Q.W., K.v.A., and J.C. acknowledge support by the Swiss National Science Foundation. Y.S. is funded by the Swedish Research Council (VR) with a Starting Grant (Dnr. 2017-05078) as well as Chalmers Area Of Advance-Materials Science. ARPES measurements were carried out at the I05 and Cassiopee beamlines of the Diamond Light Source and Soleil synchrotron, respectively.

1) F. Steglich, J. Aarts, C. D. Bredl, W. Lieke, D. Meschede, W. Franz, and H. Schäfer, Phys. Rev. Lett. **43**, 1892 (1979).
2) T. Saito, S. Onari, and H. Kontani, Phys. Rev. B **83**, 140512 (2011).
3) H. Watanabe and Y. Yanase, Phys. Rev. B **98**, 245129 (2018).
4) L. V. Pourovskii, P. Hansmann, M. Ferrero, and A. Georges, Phys. Rev. Lett. **112**, 106407 (2014).
5) O. Stockert, J. Arndt, E. Faulhaber, C. Geibel, H. S. Jeevan, S. Kirchner, M. Loewenhaupt, K. Schmalzl, W. Schmidt, Q. Si, and F. Steglich, Nat. Phys. **7**, 119 (2010).
6) J. A. Mydosh and P. M. Oppeneer, Rev. Mod. Phys. **83**, 1301 (2011).
7) S. Ghosh, M. Matty, R. Baumbach, E. D. Bauer, K. A. Modic, A. Shekhter, J. A. Mydosh, E.-A. Kim, and B. J. Ramshaw, Sci. Adv. **6**, eaaz4074 (2020).
8) J. Choi, O. Ivashko, N. Dennler, D. Aoki, K. von Arx, S. Gerber, O. Gutowski, M. H. Fischer, J. Strempfer, M. v. Zimmermann, and J. Chang, Phys. Rev. B **98**, 241113 (2018).
9) R. Daou, C. Bergemann, and S. R. Julian, Phys. Rev. Lett. **96**, 026401 (2006).
10) H. Pfau, R. Daou, M. Brando, and F. Steglich, Phys. Rev. B **85**, 035127 (2012).
11) S. Patil, A. Generalov, M. Güttler, P. Kushwaha, A. Chikina, K. Kummer, T. C. Rödel, A. F. Santander-Syro, N. Caroca-Canales, C. Geibel, S. Danzenbächer, Yu. Kucherenko, C. Laubschat, J. W. Allen, and D. V. Vyalikh, Nat. Commun. **7**, 11029 (2016).
12) S. Danzenbächer, D. V. Vyalikh, K. Kummer, C. Krellner, M. Holder, M. Höppner, Yu. Kucherenko, C. Geibel, M. Shi, L. Patthey, S. L. Molodtsov, and C. Laubschat, Phys. Rev. Lett. **107**, 267601 (2011).
13) M. Höppner, S. Seiro, A. Chikina, A. Fedorov, M. Güttler, S. Danzenbächer, A. Generalov, K. Kummer, S. Patil, S. L. Molodtsov, Y. Kucherenko, C. Geibel, V. N. Strocov, M. Shi, M. Radovic, T. Schmitt, C. Laubschat, and D. V. Vyalikh, Nat. Commun. **4**, 1646 (2013).
14) K. Kummer, S. Patil, A. Chikina, M. Güttler, M. Höppner, A. Generalov, S. Danzenbächer, S. Seiro, A. Hannaske, C. Krellner, Yu. Kucherenko, M. Shi, M. Radovic, E. Rienks, G. Zwicknagl, K. Matho, J. W. Allen, C. Laubschat, C. Geibel, and D. V. Vyalikh, Phys. Rev. X **5**, 011028 (2015).
15) S. Jang, J. D. Denlinger, J. W. Allen, V. S. Zapf, M. B. Maple, J. N. Kim, B. G. Jang, and J. H. Shim, Proc. Natl. Acad. Sci. U.S.A. **117**, 23467 (2020).
16) Q. Y. Chen, Z. F. Ding, Z. H. Zhu, C. H. P. Wen, Y. B. Huang, P.

Dudin, L. Shu, and D. L. Feng, Phys. Rev. B **101**, 045105 (2020).
17) A. F. Santander-Syro, M. Klein, F. L. Boariu, A. Nuber, P. Lejay, and F. Reinert, Nat. Phys. **5**, 637 (2009).
18) S. Danzenbächer, Yu. Kucherenko, C. Laubschat, D. V. Vyalikh, Z. Hossain, C. Geibel, X. J. Zhou, W. L. Yang, N. Mannella, Z. Hussain, Z.-X. Shen, and S. L. Molodtsov, Phys. Rev. Lett. **96**, 106402 (2006).
19) X.-G. Zhu, Y. Liu, Y.-W. Zhao, Y.-C. Wang, Y. Zhang, C. Lu, Y. Duan, D.-H. Xie, W. Feng, D. Jian, Y.-H. Wang, S.-Y. Tan, Q. Liu, W. Zhang, Y. Liu, L.-Z. Luo, X.-B. Luo, Q.-Y. Chen, H.-F. Song, and X.-C. Lai, npj Quantum Mater. **5**, 47 (2020).
20) H. J. Im, T. Ito, H.-D. Kim, S. Kimura, K. E. Lee, J. B. Hong, Y. S. Kwon, A. Yasui, and H. Yamagami, Phys. Rev. Lett. **100**, 176402 (2008).
21) Y. Wu, Y. Fang, P. Li, Z. Xiao, H. Zheng, H. Yuan, C. Cao, Y. Yang, and Y. Liu, Nat. Commun. **12**, 2520 (2021).
22) D. Ehm, S. Hüfner, F. Reinert, J. Kroha, P. Wölfle, O. Stockert, C. Geibel, and H. v. Löhneysen, Phys. Rev. B **76**, 045117 (2007).
23) M. Yano, A. Sekiyama, H. Fujiwara, Y. Amano, S. Imada, T. Muro, M. Yabashi, K. Tamasaku, A. Higashiya, T. Ishikawa, Y. Ōnuki, and S. Suga, Phys. Rev. B **77**, 035118 (2008).
24) T. Okane, T. Ohkochi, Y. Takeda, S.-i. Fujimori, A. Yasui, Y. Saitoh, H. Yamagami, A. Fujimori, Y. Matsumoto, M. Sugi, N. Kimura, T. Komatsubara, and H. Aoki, Phys. Rev. Lett. **102**, 216401 (2009).
25) A. Vittorini-Orgeas and A. Bianconi, J. Supercond. Novel Magn. **22**, 215 (2009).
26) J. D. Denlinger, G.-H. Gweon, J. W. Allen, C. G. Olson, M. B. Maple, J. L. Sarrao, P. E. Armstrong, Z. Fisk, and H. Yamagami, J. Electron Spectrosc. Relat. Phenom. **117–118**, 347 (2001).
27) M. Hoesch, T. K. Kim, P. Dudin, H. Wang, S. Scott, P. Harris, S. Patel, M. Matthews, D. Hawkins, S. G. Alcock, T. Richter, J. J. Mudd, M. Basham, L. Pratt, P. Leicester, E. C. Longhi, A. Tamai, and F. Baumberger, Rev. Sci. Instrum. **88**, 013106 (2017).
28) M. Horio, K. Hauser, Y. Sassa, Z. Mingazheva, D. Sutter, K. Kramer, A. Cook, E. Nocerino, O. K. Forslund, O. Tjernberg, M. Kobayashi, A. Chikina, N. B. M. Schröter, J. A. Krieger, T. Schmitt, V. N. Strocov, S. Pyon, T. Takayama, H. Takagi, O. J. Lipscombe, S. M. Hayden, M. Ishikado, H. Eisaki, T. Neupert, M. Månsson, C. E. Matt, and J. Chang, Phys. Rev. Lett. **121**, 077004 (2018).
29) Y.-M. Xu, Y.-B. Huang, X.-Y. Cui, E. Razzoli, M. Radovic, M. Shi, G.-F. Chen, P. Zheng, N.-L. Wang, C.-L. Zhang, P.-C. Dai, J.-P. Hu, Z. Wang, and H. Ding, Nat. Phys. **7**, 198 (2011).
30) P. Vilmercati, A. Fedorov, I. Vobornik, U. Manju, G. Panaccione, A. Goldoni, A. S. Sefat, M. A. McGuire, B. C. Sales, R. Jin, D. Mandrus, D. J. Singh, and N. Mannella, Phys. Rev. B **79**, 220503 (2009).
31) K. Kramer and J. Chang, J. Open Source Softw. **6**, 2969 (2021).
32) (Supplemental Material) More detailed discussions and observations on the Brillouin zone and about other potential causes for the observed experimental results in the temperature dependence can be found online.
33) K. Kummer, Yu. Kucherenko, S. Danzenbächer, C. Krellner, C. Geibel, M. G. Holder, L. V. Bekenov, T. Muro, Y. Kato, T. Kinoshita, S. Huotari, L. Simonelli, S. L. Molodtsov, C. Laubschat, and D. V. Vyalikh, Phys. Rev. B **84**, 245114 (2011).
34) J. D. Denlinger, J.-S. Kang, L. Dudy, J. W. Allen, K. Kim, J.-H. Shim, K. Haule, J. L. Sarrao, N. P. Butch, and M. B. Maple, Electron. Struct. **4**, 013001 (2022).
35) C. Bareille, F. L. Boariu, H. Schwab, P. Lejay, F. Reinert, and A. F. Santander-Syro, Nat. Commun. **5**, 4326 (2014).
36) T. J. Nummy, J. A. Waugh, P. S. Parham, Q. Liu, H.-Y. Yang, H. Li, X. Zhou, N. C. Plumb, F. F. Tafti, and D. S. Dessau, npj Quantum Mater. **3**, 24 (2018).
37) M. Horio, C. E. Matt, K. Kramer, D. Sutter, A. M. Cook, Y. Sassa, K. Hauser, M. Månsson, N. C. Plumb, M. Shi, O. J. Lipscombe, S. M. Hayden, T. Neupert, and J. Chang, Nat. Commun. **9**, 3252 (2018).
38) A. Damascelli, Z. Hussain, and Z.-X. Shen, Rev. Mod. Phys. **75**, 473 (2003).
39) T. Willers, F. Strigari, N. Hiraoka, Y. Q. Cai, M. W. Haverkort, K.-D. Tsuei, Y. F. Liao, S. Seiro, C. Geibel, F. Steglich, L. H. Tjeng, and A. Severing, Phys. Rev. Lett. **109**, 046401 (2012).
40) H. Yamagami and A. Hasegawa, J. Phys. Soc. Jpn. **61**, 2388 (1992).
41) J. C. Slater and G. F. Koster, Phys. Rev. **94**, 1498 (1954).
42) K. Takegahara, Y. Aoki, and A. Yanase, J. Phys. C **13**, 583 (1980).
43) P. Haen, J. Flouquet, F. Lapierre, P. Lejay, and G. Remenyi, J. Low Temp. Phys. **67**, 391 (1987).
44) Y. Shimizu, Y. Matsumoto, K. Aoki, N. Kimura, and H. Aoki, J. Phys. Soc. Jpn. **81**, 044707 (2012).
45) A. Koizumi, G. Motoyama, Y. Kubo, T. Tanaka, M. Itou, and Y. Sakurai, Phys. Rev. Lett. **106**, 136401 (2011).
46) Z. Wu, Y. Fang, H. Su, W. Xie, P. Li, Y. Wu, Y. Huang, D. Shen, B. Thiagarajan, J. Adell, C. Cao, H. Yuan, F. Steglich, and Y. Liu, Phys. Rev. Lett. **127**, 067002 (2021).
47) S. A. Grigera, P. Gegenwart, R. A. Borzi, F. Weickert, A. J. Schofield, R. S. Perry, T. Tayama, T. Sakakibara, Y. Maeno, A. G. Green, and A. P. Mackenzie, Science **306**, 1154 (2004).
48) P. A. Lee, N. Nagaosa, and X.-G. Wen, Rev. Mod. Phys. **78**, 17 (2006).
49) A. W. Rost, R. S. Perry, J.-F. Mercure, A. P. Mackenzie, and S. A. Grigera, Science **325**, 1360 (2009).
50) Y. Xu, F. Herman, V. Granata, D. Destraz, L. Das, J. Vonka, S. Gerber, J. Spring, M. Gibert, A. Schilling, X. Zhang, S. Li, R. Fittipaldi, M. H. Fischer, A. Vecchione, and J. Chang, Commun. Phys. **4**, 1 (2021).